# Structure of the MUR1 GDP-Mannose 4,6-Dehydratase from *Arabidopsis thaliana*: Implications for Ligand Binding and Specificity

Anne M. Mulichak,[‡] Christopher P. Bonin,[§,||] Wolf-Dieter Reiter,[§] and R. Michael Garavito*[,‡]

*Department of Biochemistry and Molecular Biology, Michigan State University, East Lansing, Michigan 48824-1319, and Department of Molecular and Cell Biology, University of Connecticut, Storrs, Connecticut 06269*

*Received August 19, 2002*

ABSTRACT: GDP-D-mannose 4,6-dehydratase catalyzes the first step in the de novo synthesis of GDP-L-fucose, the activated form of L-fucose, which is a component of glycoconjugates in plants known to be important to the development and strength of stem tissues. We have determined the three-dimensional structure of the MUR1 dehydratase isoform from *Arabidopsis thaliana* complexed with its NADPH cofactor as well as with the ligands GDP and GDP-D-rhamnose. MUR1 is a member of the nucleoside-diphosphosugar modifying subclass of the short-chain dehydrogenase/reductase enzyme family, having homologous structures and a conserved catalytic triad of Lys, Tyr, and Ser/Thr residues. MUR1 is the first member of this subfamily to be observed as a tetramer, the interface of which reveals a close and intimate overlap of neighboring $NADP^+$-binding sites. The GDP moiety of the substrate also binds in an unusual syn conformation. The protein−ligand interactions around the hexose moiety of the substrate support the importance of the conserved triad residues and an additional Glu side chain serving as a general base for catalysis. Phe and Arg side chains close to the hexose ring may serve to confer substrate specificity at the O2 position. In the MUR1/GDP-D-rhamnose complex, a single unique monomer within the protein tetramer that has an unoccupied substrate site highlights the conformational changes that accompany substrate binding and may suggest the existence of negative cooperativity in MUR1 function.

The 6-deoxy monosaccharide L-fucose is found as a component of glycoconjugates in organisms from bacteria to mammals and has a diverse range of functions. In humans, L-fucose is most notably an important constituent of glycoproteins such as the blood group antigens as well as cell surface carbohydrate ligands of the cell adhesion family of selectins involved in functions such as inflammation and the immune response (*1*). Among other organisms, L-fucose-containing glycoconjugates are involved in developmental signaling in *Drosophila* (*2*), are critical components of bacterial cell walls where they may play a role in pathogenicity, and among rhizobial organisms, are components of Nod factors, influencing nodulation efficiency and host specificity (*3*, *4*). In plants, L-fucose has important structural functions as a component of glycoproteins and cell wall polysaccharides, such as xyloglucan and rhamnogalacturonans I and II. Xyloglucan molecules cross-link cellulose microfibrils, one of the major load-bearing elements of the cell wall, and may be involved in the regulation of extension growth. It has been proposed that L-fucose may stabilize conformations that effectively bind cellulose (*5*, *6*); however, this hypothesis has recently been challenged on the basis of the normal growth habit and wall strength of an *Arabidopsis* mutant specifically deficient in xyloglucan fucosylation (*7*). Although the function of rhamnogalacturonan II is unknown, the presence of fucose appears to be important for formation of the normal borate di-ester cross-linked form of this polysaccharide (*8*).

L-Fucose is incorporated into these glycoconjugates from the activated donor form, GDP-L-fucose. In all organisms studied thus far, the de novo biosynthesis of GDP-L-fucose occurs via a conserved, two-step biosynthetic pathway (Figure 1): the formation of GDP-4-keto-6-deoxy-D-mannose from GDP-D-mannose, which is catalyzed by the enzyme GDP-mannose 4,6-dehydratase (GMD), followed by epimerization and reduction reactions catalyzed by a second enzyme to form the GDP-L-fucose product.

Enzymes having GMD activity have been identified in diverse organisms, including bacteria, plants, and mammals. GMDs are highly similar in amino acid sequences and belong to a sugar-modifying subclass of the NAD(P)-dependent short-chain dehydrogenase/reductase (SDR) family of enzymes (*9*−*13*). SDRs have quite homologous three-dimensional structures and share a small number of highly conserved amino acids, including a triad of Tyr-XXX-Lys and Ser/Thr residues that are important for catalysis. The three-dimensional structures of several enzymes from this subfamily have been determined by X-ray crystallography (*14*−*22*), including the GMD from *Escherichia coli* (*23*). Of the closely related enzymes, UDP-galactose epimerase (GalE) and dTP-glucose 4,6-dehydratase (dTGDH) have been

* To whom correspondence should be addressed. E-mail: garavito@msu.edu. Phone: (517)355-9724. Fax: (517)353-9334.

[‡] Michigan State University.

[§] University of Connecticut.

[||] Present address: Department of Biochemistry and Molecular Biophysics, Columbia University, New York, NY 10032.

[1] Abbreviations: dTGDH, dTDP-glucose 4,6-dehydratase; GalE, UDP-galactose epimerase; GMD, GDP-D-mannose 4,6-dehydratase; SDR, short-chain dehydrogenase/reductase.

10.1021/bi0266683 CCC: $22.00 
Published on Web 11/26/2002

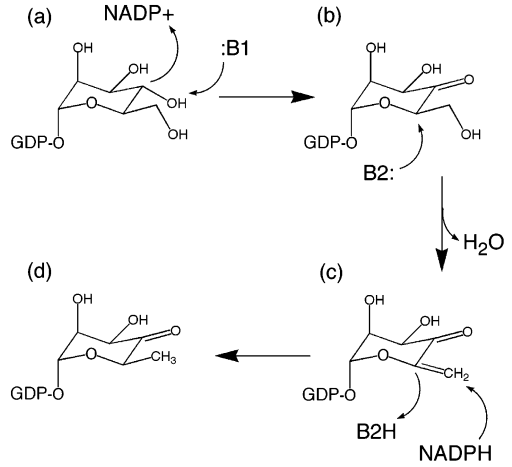


FIGURE 1: Schematic diagram of the mechanism proposed for catalysis by GDP-mannose dehydratase, whereby GDP-mannose (a) is converted to GDP-4-keto-6-deoxymannose (d) via 4-keto (b) and 4-keto-5,6-ene (c) intermediates.

investigated extensively by crystallographic (*15*, *16*, *19*, *24*−*31*), mutagenesis and kinetic (*32*−*49*) studies.

In *Arabidopsis thaliana*, two isoforms of GDP-mannose dehydratase, having 92% amino acid sequence identity, have been identified: MUR1, which is expressed throughout the plant tissues, and GMD1, which appears to be root-specific (*50*). Mutations of the *mur1* gene produce plants with a nearly complete deficiency of fucose in above-ground tissues and a 40% reduction of fucose in root tissue. Although L-fucose may be replaced by L-galactose to some extent (*51*), *mur1* plants are characterized by markedly dwarfed growth and compromised tensile stem strength (*52*). The recent structure of *apo*-GMD from *E. coli* (*23*) established its general tertiary structure, but the absence of crystal structures with bound cofactor or substrate provided little insight into the mechanisms of ligand binding and catalysis. To investigate these issues, we have determined the X-ray crystal structure of the MUR1 enzyme in complexes with the NADP(H) cofactor as well as GDP and GDP-rhamnose, a byproduct formed from the natural MUR1 GDP-4-keto-6-deoxy-D-mannose product during overexpression. The MUR1 structure also reveals ligand-induced conformational changes, a novel oligomeric state among enzymes of this family, and an unexpected conformation for the bound nucleotide-sugar substrate.

## EXPERIMENTAL PROCEDURES

*Expression and Purification.* The *mur1* gene was cloned into a pET28b vector (Novagen), adding a Leu-Glu sequence and hexahistidine tag at the C-terminus, and transformed into *E. coli* expression strain BL21(DE3). Starting cultures (100 mL) were grown overnight at 37 °C from glycerol stocks. Several 1-L cultures were then grown at 37 °C until 0.5−0.6 o.d. at 600 nm was reached. The cultures were then induced with 0.12 mM IPTG and grown at room temperature for 16 h. Harvested cells were lysed by sonication in buffer A (50 mM HEPES, 300 mM NaCl, and 2 mM $\beta$-mercaptoethanol at pH 8.0) and centrifuged at 10000*g* for 30 min to remove cell debris. The resulting supernatant fraction was loaded onto an Ni−NTA column (Qiagen), washed with buffer B (50 mM HEPES, 300 mM NaCl, 2 mM $\beta$-mercaptoethanol, and 20 mM imidazole at pH 7.5), and eluted with a buffer similar to buffer B but having 200 mM imidazole. Selenomethionine (Se-Met) labeled MUR1 was prepared by growing *E. coli* BL21(DE3) initially in LB media, followed by transfer into minimal media supplemented with L-selenomethionine (Anatrace, Inc., Maumee, OH). Se-Met-labeled MUR1 was isolated and purified following the same protocol used on the native protein.

*Crystallization.* The purified MUR1 enzyme was crystallized using the hanging drop vapor diffusion method: the protein was mixed with a reservoir solution in a 1:1 volume ratio, and the resulting droplet was placed against the undiluted reservoir solution. Crystallization screening experiments based on the sparse matrix methodology (*53*) were performed, in the presence and absence of ligands, to identify conditions that supported crystal growth. In the absence of any added NADP(H) cofactor or substrate, prismatic crystals grew in ~2.1 M ammonium sulfate, 2−2.5% (w/v) PEG 400, and 0.1 M imidazole buffer (pH 6.4). These type I crystals belong to the space group $P2_12_12_1$ ($a$ = 113.2 Å, $b$ = 119.0 Å, $c$ = 118.9 Å) and contain four protein molecules per asymmetric unit. In the presence of 2 mM NADPH and 10 mM GDP, crystals of similar morphology were obtained under identical conditions. However, this type II crystal form belong to the related space group $C222_1$ ($a$ = 116.9 Å, $b$ = 124.7 Å, $c$ = 110.6 Å) and has two molecules per asymmetric unit. Se-Met-labeled MUR1, in the presence of 2 mM NADPH, was also crystallized under reservoir conditions similar to those used to grow type I crystals. In this case, the optimized crystallization conditions for the Se-Met-substituted protein required the addition of 0.5% $\beta$-octyl glucoside to minimize crystal growth defects. The resulting crystals, hexagonal bipyramids, belongs to space group $P6_222$ ($a = b$ = 98.0 Å, $c$ = 150.2 Å) with one molecule in the asymmetric unit. Prior to data collection, all crystals were transferred to a solution similar to the reservoir conditions for growth but supplemented with 30% glycerol as a cryoprotectant and flash-frozen in liquid propane. To prevent cracking of the crystals, transfer to cryo conditions was performed incrementally, increasing the glycerol concentration in steps of 5% at intervals of 1 min.

*Data Collection.* Multiwavelength anomalous X-ray diffraction data at 3.5 Å resolution were collected from Se-Met-labeled MUR1 crystals at the Structural Biology Center beamline 19-ID at the Advanced Photon Source, Argonne National Laboratory. Four data sets were measured at the selenium K-absorption edge peak (0.9793 Å), inflection point (0.9795 Å), and high (0.9464 Å) and low (1.01626 Å) energy remote wavelengths. Data were processed using HKL2000 and scaled using SCALEPACK software (*54*).

For the type I crystal form of the native MUR1 enzyme, data at 2.2 Å resolution were collected at the Advanced Photon Source beamline 5-ID (DND-CAT) at 100° K on a MAR CCD detector using radiation at 1.0 Å wavelength. For the MUR1 ternary complex with NADPH and GDP (type II crystals), a 1.8 Å resolution data set was measured at the National Synchrotron Light Source beamline X-25 at 95 K on a Brandeis B4 area detector and using radiation at 1.1 Å wavelength. Both latter data sets were integrated and scaled using HKL version 1.96.6 software (*54*). The statistics of data collection for the three crystal forms are summarized in Table 1.

Table 1: Statistics of X-ray Data Collection

| data set | space group | resoln (Å) | unique reflns | completeness (%) | $R_{merge}$[a] |
|---|---|---|---|---|---|
| MUR1 type I | $P2_12_12_1$ | 2.2 | 76177 | 92 (78)[b] | 3.8 (20.2) |
| MUR1 type II | $C222_1$ | 1.8 | 70780 | 95 (88) | 6.2 (7.7) |
| SeMet-MUR1 | $P6_522$ | | | | |
| peak | | 3.2 | 13242 | 100 (100) | 7.6 (31.9) |
| inflection | | 3.2 | 13265 | 100 (100) | 8.2 (31.5) |
| low remote | | 3.2 | 13299 | 100 (100) | 7.9 (31.7) |
| high remote | | 3.2 | 13262 | 100 (100) | 8.1 (32.0) |

[a] $R_{merge} = \sum|I - \langle I\rangle|/\sum I$, where $I$ is the observed intensity of an individual reflection, and $\langle I\rangle$ is the mean intensity of that reflection. [b] Values in parentheses represent values in last shell.

*Phasing and Structure Refinement.* Despite its moderate resolution limit, the hexagonal Se-MUR1 crystal form was suitable for phasing using multiwavelength anomalous dispersion methods. CNSsolve v0.9a (*55*) was used to determine 6 of 8 Met positions for the hexagonal Se-MUR1 crystal form, producing initial phases at 3.5 Å resolution having an overall figure of merit value of 0.78. Phases were improved through density modification using density truncation and solvent flipping techniques, yielding a final figure of merit of 0.87. Although the initial MAD phased electron density maps were not of high quality, they were sufficient to position a model based on the known structures of homologous enzymes. Chain interactive graphics software (*56*) was then used to build a MUR1 model containing one protein molecule and one bound NADPH molecule in the asymmetric unit. The structure was partially refined at 3.2 Å resolution against the low-energy remote wavelength data set using CNSsolve v0.9a software with an overall B-factor to a *R*-factor of 0.254 (*R*-free = 0.339).

The resulting atomic model of Se-MUR1/NADPH complex was then used for molecular replacement phasing of the types I and II MUR1 crystals using the AMoRe programs (*57*) in the CCP4 crystallographic program suite (*58*). The atomic models for both orthorhombic crystal forms were refined using similar strategies. Using CNSsolve v0.9a, several initial cycles of simulated annealing were followed by simple positional refinement; each refinement cycle alternated with a cycle of manual model-building using Chain interactive graphics software. Noncrystallographic symmetry restraints were imposed between the two independent monomers of the type II form; in the asymmetric unit of the type I crystals, similar restraints were imposed between the three equivalent molecules. In later stages, individual B-factors were refined, and water molecules were included in the models at positions having $|F_o - F_c|$ electron density above the $3\sigma$ level and appropriate geometry to a hydrogen-bonding partner. In the type I crystal structure, electron density clearly indicated the presence of bound NADPH in all independent monomers as well as a GDP-sugar ligand bound to three of the four subunits, *despite* the absence of any added ligands in the crystallization conditions. The final type I model ($R_{factor} = 0.201$, $R_{free} = 0.247$) includes a MUR1 tetramer with four bound NADPH molecules, three bound GDP-D-rhamnose molecules, and 475 water molecules. For the type II crystal structure, good electron density was observed for bound NADPH cofactors as well as for bound GDP. The final type II model ($R_{factor} = 0.180$, $R_{free} = 0.200$) includes an independent dimer of the MUR1 tetramer, one NADPH and one GDP in each monomer, and 440 water molecules. For both crystal forms, the MUR1 models generally include residues 28−367 of 373 possible amino acids and contain a short 6−8 residue break in the main chain occurring at approximately residue 76. The single unique monomer of the type I crystal form has two additional disordered regions at segments 246−250 and 310−318, and the C-terminus is only observed to residue 362. Refinement results for both crystal forms are summarized in Table 2. The atomic coordinates and structure factors for the MUR1/NADPH/GDP-D-rhamnose (type I) and the MUR1/NADPH/GDP (type II) crystal structures have been deposited in the Protein Data Bank as entries 1N7G and 1N7H, respectively.

Table 2: Statistics of Structure Refinement

| data set | type I | type II |
|---|---|---|
| resolution (Å) | 30−2.2 | 10−1.8 |
| total atoms | 11035 | 5761 |
| | 4 MUR1 | 2 MUR1 |
| | 4 NADPH | 2 NADPH |
| | 3 GDP-D-rhamnose | 2 GDP |
| | 475 waters | 440 waters |
| reflections | | |
| working set | 68,520 | 66,421 |
| test set | 3,521 | 3,557 |
| *R*-factor[a] (%) | 20.1 | 18.0 |
| *R*-free[b] | 24.7 | 20.1 |
| rmsd[c] | | |
| bonds (Å) | 0.005 | 0.006 |
| angles (deg) | 1.2 | 1.4 |
| dihedrals (deg) | 23 | 23 |
| impropers (deg) | 0.8 | 1.0 |

[a] *R*-factor = $\sum|F_o - F_c|/\sum F_o$, where $F_o$ and $F_c$ are observed and calculated structure factors, respectively. [b] *R*-free is the cross validation *R*-factor computed for the test set of reflections (5% of the total were used). [c] rmsd is the root-mean-square deviation.

## RESULTS AND DISCUSSION

*General Structure and Oligomeric State.* As expected, MUR1 has a bi-domain structure (Figure 2), observed in the known structures of the *E. coli* GMD (*23*) and other related NDP-sugar modifying SDRs. The core of the large domain, which is responsible for binding the NADP(H) cofactor, is comprised of a Rossmann fold, a motif of parallel $\beta$-sheet interleaved by flanking α-helices that is commonly associated with dinucleotide binding sites. As is characteristic for all enzymes of the SDR family, the sixth and typically final $\beta$-strand of the canonical Rossmann fold motif is followed by a peptide extension that adds a seventh $\beta$-strand and additional long connecting α-helix. In GMD, as well as other more closely related NDP-sugar modifying enzymes, this C-terminal portion is greatly elaborated to form a distinct second small domain, which binds the sugar-nucleotide substrate. The small domain is formed largely of a bundle of three α-helices with a short section of mixed parallel and antiparallel $\beta$-sheet.

In all three crystal forms, which represent crystal lattices with one, two, and four protein molecules per asymmetric unit, the MUR1 enzyme is found to be a homotetramer having 222 molecular symmetry (Figure 2b). Gel filtration results (data not shown) are consistent with the hypothesis that the MUR1 tetramer exists in solution and is not a crystallization artifact. This is the first direct observation of

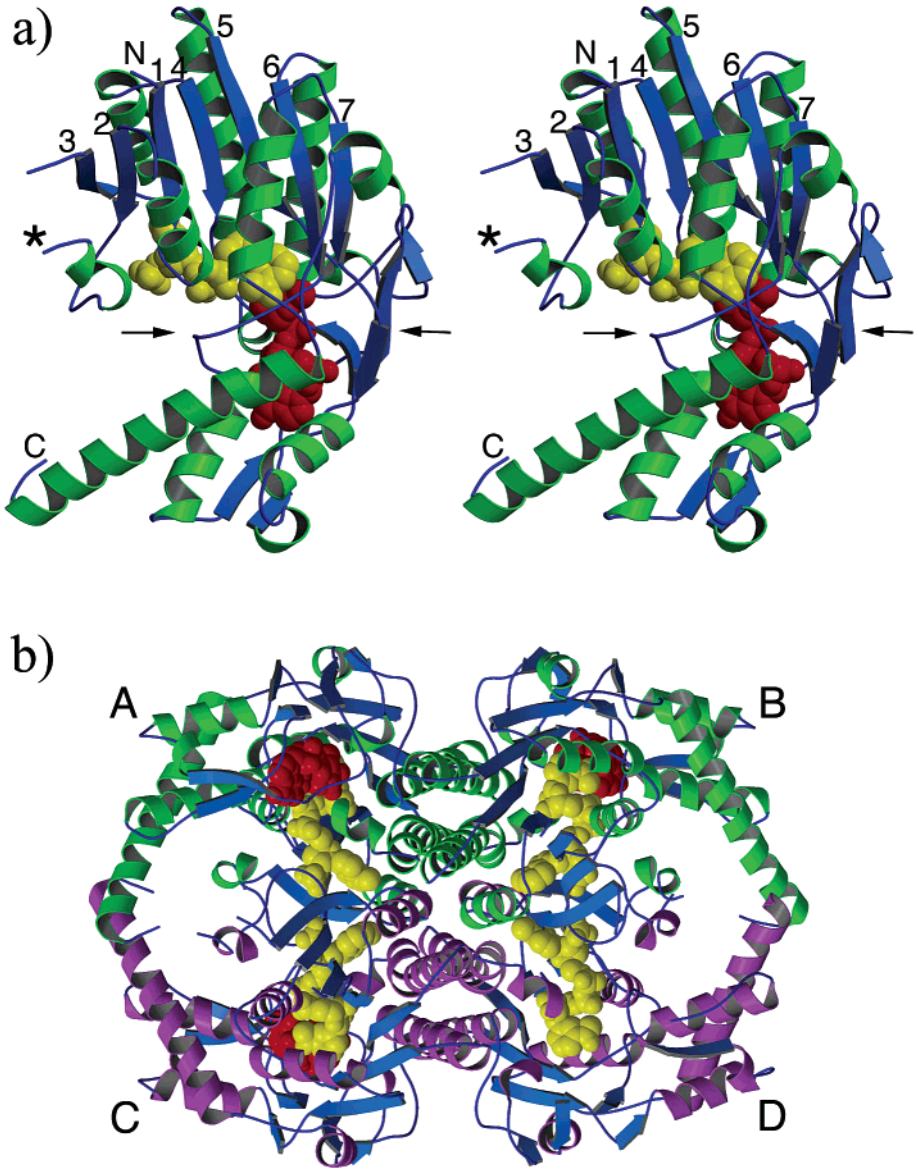


FIGURE 2: Ribbon drawings showing structures of (a) the MUR1 monomer in stereoview and (b) the arrangement of four MUR1 molecules (A−D) to form a tetramer. For the monomer, secondary structure is highlighted by color, the $\beta$-strands of the Rossmann motif are numbered consecutively, and an asterisk indicates the disordered peptide 76−81. The positions of bound NADPH (yellow) and GDP-D-rhamnose (red) molecules are shown as space-filling models. Arrows indicate the boundary between the large (above) and the small (below) domains. In panel b, helices in green and violet differentiate the two characteristic SDR dimers that combine to form the MUR1 tetramer. Within the tetramer, one MUR1 monomer (D) is unique in having an unoccupied substrate binding site. Figure was prepared using Molscript (*72*) and Raster3D (*73*).

a tetramer among the enzymes of the nucleotide-sugar modifying SDR subfamily. Moreover, the observed crystal forms for MUR1 demonstrate that the tetramer can assume perfect 222 crystallographic symmetry (i.e., all subunits assume the same conformational state) or can break the 222 molecular symmetry as seen in the type I crystals (see below).

Within the MUR1 tetramer, two monomers are associated by a back-to-back packing interface in which the two long parallel $\alpha$4 and $\alpha$5 helices of the large domains from each monomer form an extensive, four-helix bundle. With the exceptions of ADP-L-glycero-D-mannoheptose 6-epimerase (*20*) and dTDP-6-deoxy-L-lyxo-4-hexulose reductase (*21*), this dimer interface is found in all structures of closely related enzymes as well as in nearly all other SDR enzymes. Two canonical "SDR dimers" then combine to form the MUR1 tetramer, creating an extended interface of parallel helices and burying approximately 3100 Å$^2$ of accessible surface area of each dimer. At the dimer−dimer interface, the dinucleotide binding clefts of neighboring monomers abut against each other, such that the adenosyl phosphate moieties of bound NADPH molecules are within 7.5 Å (Figure 3). The cofactor binding sites of the two monomers are intimately overlapped in this region (as discussed below). However, the region around the nicotinamide ring and adjacent substrate binding site remain accessible and unaffected by tetramer formation.

Among the crystal structures of the more distantly related SDRs, many are observed to be homotetramers that incorporate the same conserved dimer interface as the dimeric family members. However, the dimer−dimer interactions in these tetramers are not equivalent to those found in MUR1. This situation is analogous to the NAD-linked dehydrogenases (*59*) where two different modes for tetramer formation exist: one that produces noninteracting binding sites (e.g.,

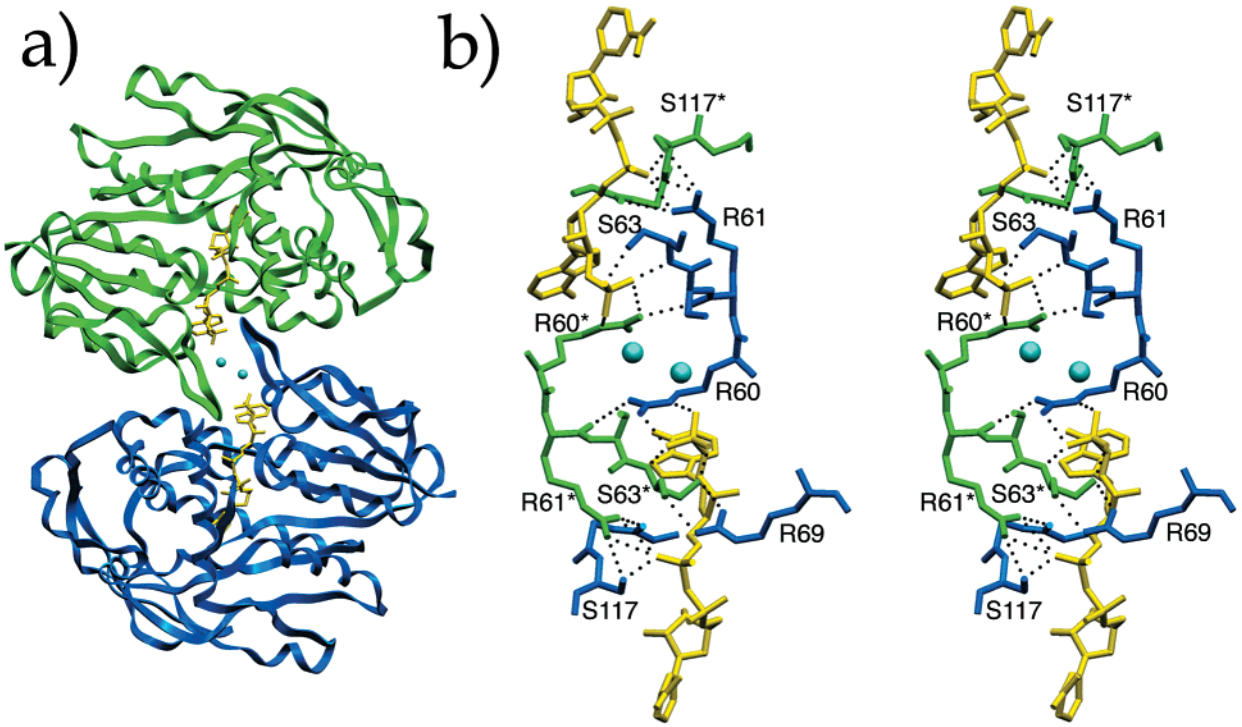


FIGURE 3: (a) View of the novel MUR1 tetramer interface where loops 60−69 of two monomers, shown in blue and green, extend to make several hydrogen-bonding interactions with the opposite protein molecule as well as with its bound NADPH cofactor (yellow). Water molecules that bridge the NADPH phosphate moieties are depicted as blue spheres. (b) Stereoview showing detail of the overlapping NADPH binding sites. Dashed lines indicate potential hydrogen bonds. For clarity, not all protein−protein interactions between the 60−69 loops are shown. Figures 4−6 were prepared using SETOR (*74*).

lactate dehydrogenase) and another that permits cooperative interactions (e.g., glyceraldehyde 3-phosphate dehydrogenase). The extensive interactions between the NADP(H) binding sites observed in the MUR1 tetramer clearly suggest that a dimer−tetramer transition might occur in many GMDs and may be dependent on NADP(H) binding. Interestingly, the apo-form of *E. coli* GMD was found to be a dimer in the crystal structure and in solution (*23*). Moreover, recombinant human GMD depleted of NADP(H) was also found to be mainly a dimer (*60*). On the other hand, larger oligomeric species of GMD were observed in *H. pylori* (*61*), in porcine thyroid (*62*), and even in *E. coli* when a sufficient amount of NADP(H) remained bound (*63*). The flattened and elongated ellipsoidal shape (~100 Å × 74 Å × 57 Å) of the MUR1 tetramer may explain the larger oligomeric sizes seen for GMD complexed with NADP(H).

In the MUR1/NADPH/GDP complex (type II crystals), both independent monomers bind GDP; in the type I crystal form, three monomers in the asymmetric unit contain a bound GDP-sugar. The enzyme conformation of the MUR1 molecules containing bound GDP or a GDP-sugar is virtually identical (~0.35 Å rmsd on main-chain atoms). These MUR1 molecules each include residues 28−366, with a small break in the main chain where residues 76−81 are disordered and unobserved in electron density maps. This disordered segment immediately precedes the $\beta$3 strand of the Rossmann fold, in a loop which is highly variable in both size and amino acid sequence among the enzymes of the nucleotide-sugar modifying SDR subfamily. The GDP-sugar binding site of the fourth monomer in the asymmetric unit of the type I crystals is unoccupied. This "empty" monomer differs significantly in conformation from the other three monomers of the tetramer in the type I crystals, with a rmsd of approximately 1 Å overall in the main-chain atoms (discussed in more detail below). Although the molecular packing within the $C222_1$ and $P2_12_12_1$ crystal lattices is equivalent, the type I $P2_12_12_1$ crystal lattice allows the breakdown of the 222 molecular symmetry tetramer with only minor changes in crystal contacts.

Generally, the structure of MUR1 corresponds well with that of the apo *E. coli* GMD (*23*), where a slightly better agreement (rmsd of 1.1 Å on Cα atoms) occurs with the MUR1 monomer that also lacks bound substrate. The conformations of the small, substrate-binding domains are most variable overall between the two structures and include a large peptide insertion in the *E. coli* enzyme; however, the position of the three α-helix bundle remains reasonably well conserved. The large domains superimpose more closely (0.8 Å rmsd) with two notable exceptions that arise from the differences in NADP(H) binding and oligomerization state. The first significant difference is the loop formed by residues 60−75, which makes interactions important for both NADP(H) binding and tetramer formation in the MUR1 structures but is completely disordered in the *E. coli apo*-GMD. The second is a large deviation in the loop following the $\beta$4 strand (MUR1 residues 114−124), which forms part of the cofactor binding cleft. In the *E. coli* GMD structure this loop is shifted by up to 9 Å and partially occupies the position of bound cofactor. The α4 helix, which immediately follows this segment, is also shifted by approximately 1.3 Å. Thus, cofactor binding appears to be critical both for tetramer formation and to induce the active conformation of the GMD enzymes.

*Cofactor Binding.* All GMDs studied thus far are known to utilize $NADP^+$ exclusively or preferentially over $NAD^+$. The MUR1 crystal structures reveal well-ordered NADPH

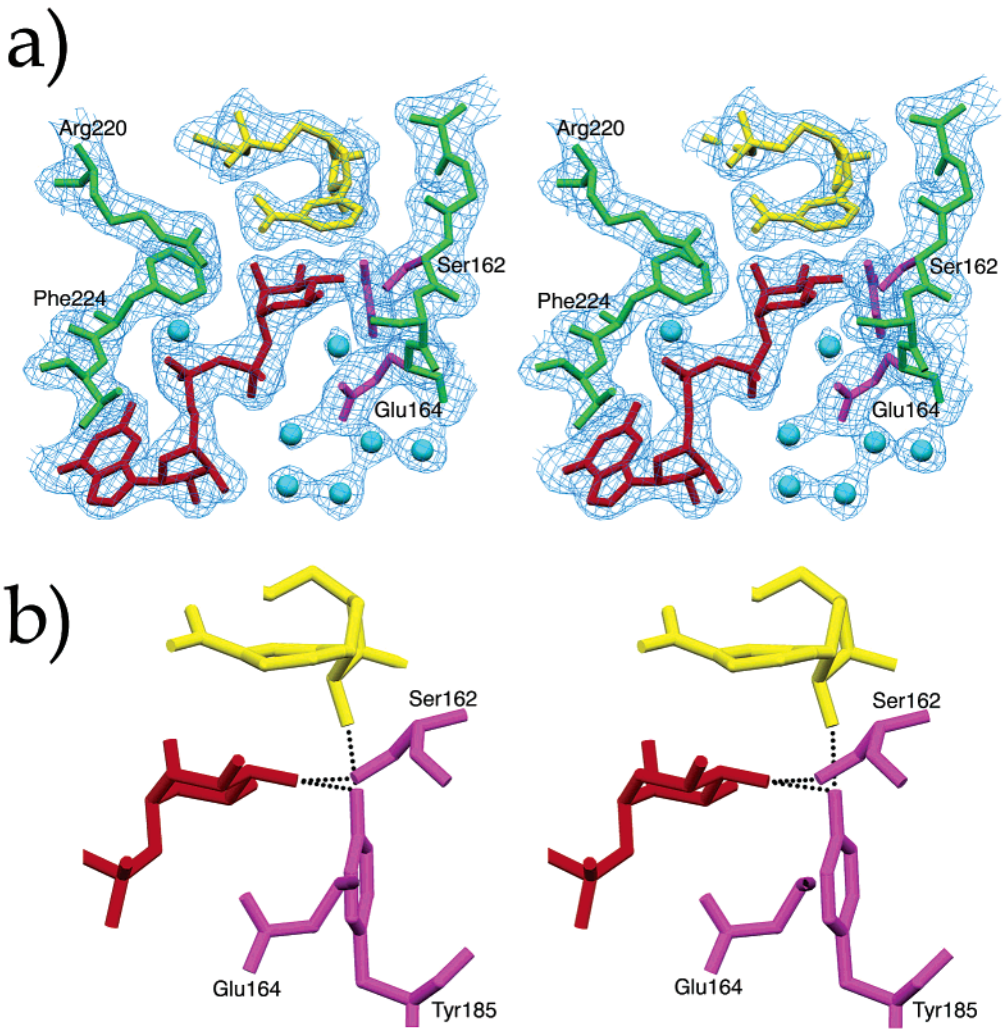


FIGURE 4: (a) Stereoview showing $2F_o - F_c$ electron density ($1\sigma$ level) at the MUR1 active site with GDP-D-rhamnose (red) and NADPH (yellow) bound. Catalytic residues are highlighted in magenta, and spheres represent buried water molecules. (b) Stereoview illustrating the detailed interactions between the MUR1 catalytic residues, substrate hexose, and cofactor nicotinamide moieties. Dashed lines indicate hydrogen bonds. The nicotinamide C4 atom is positioned midway between the hexose C4 and C6 atoms, the donor and acceptor positions of hydride transfer, respectively.

molecules bound in all monomers, even when no cofactor was included in crystallization experiments, demonstrating that the cofactor remains tightly bound to the MUR1 enzyme throughout purification. The observed nonplanar electron density at the nicotinamide moiety (Figure 4) is consistent with the reduced form of the cofactor ring. The conformation of bound NADPH is identical in all the MUR1 structures determined, regardless of whether GDP, GDP-sugar, or no ligand at all is bound to the enzyme. This is in contrast to crystallographic studies of GalE, which found the conformation of the cofactor to vary depending on oxidation state and the presence or absence of a sugar moiety in the substrate binding site (*16*, *24*). Attempts to exchange the NADPH bound in MUR1 by cocrystallization with excess $NADP^+$ or NAD(H) were unsuccessful; the reduced NADPH cofactor was still clearly observed in electron density maps.

Binding interactions of the cofactor in the MUR1 binding site are shown schematically in Figure 5. Consistent with previous homologous structures, the NADPH cofactor binds in an extended conformation to the MUR1 large domain, with the pyrophosphate bridge positioned at the N-terminal end (or positive dipole) of the α1 helix, in a manner characteristic of the Rossmann dinucleotide-binding motif. The glycine-rich signature sequence of the classical Rossmann motif, Gly35-XX-Gly38-XX-Gly41 (where X is any amino acid) allows a close approach of the cofactor with the enzyme backbone with direct hydrogen-bonds formed between the pyrophosphate and the amide nitrogen atoms of Gln39 and Asp40. Additional hydrogen bonds are provided to the pyrophosphate by the side chains of Ser117 and Arg220.

The most striking feature of the MUR1 cofactor binding site is that it, as well as the bound NADPH itself, is an integral and intimate part of the tetramer interface that completely buries the adenosyl phosphate portion of the bound cofactor (Figure 3). Interactions at this interface are formed predominantly by the peptide segment Arg60-Arg69, part of the loop between the large domain $\beta$2 strand and α2 helix, just preceding the disordered region at Asp76-Asn81. This loop, highly variable in size and amino acid sequence among related enzymes, closes over the adenosyl end of bound cofactor in the structures of several other NAD-binding homologues. In the MUR1 tetramer, the Arg60-Arg69 loops from adjacent monomers instead extend across the dimer−dimer interface to interact with each other in a symmetric "fireman's grip" manner. The two Arg60 side

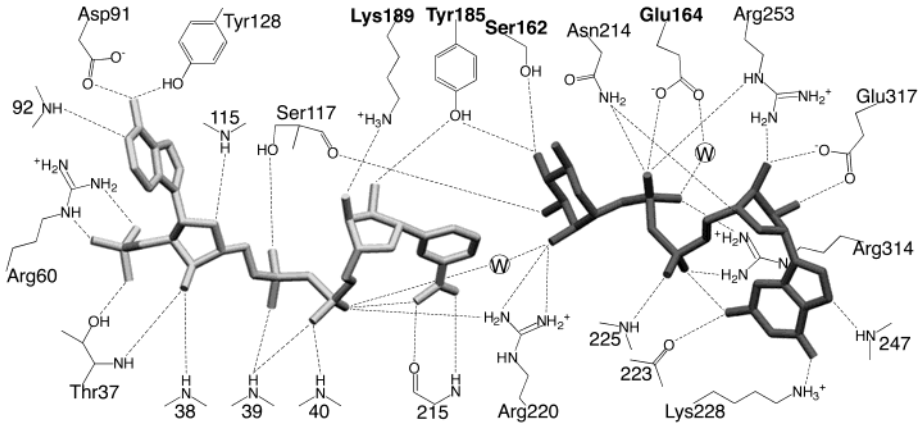


FIGURE 5: Schematic diagram of potential hydrogen-bonding interactions (dashed lines) of bound NADPH and GDP-D-rhamnose with MUR1 binding site. For clarity, interactions of NADPH with residues from the neighboring MUR1 monomer and some water molecules (W) are not included.

chains adopt a nearly parallel stacked arrangement, with a planar separation of approximately 4.5 Å. A number of direct interactions are formed between the two loops, including hydrogen bonds between the side chains of Arg60, Asn64, and Arg69 with the main-chain carbonyl oxygen atoms of Arg61*, Asn66*, and Ser63*, respectively, from the second monomer. The Arg69 side chain simultaneously forms a hydrogen bond with the Ser63* side chain hydroxyl as well.

Although the loops participate somewhat in cofactor binding within the same monomer via hydrogen-bonding of the Arg60 side chain to the adenosyl phosphate moiety, they actually contribute more extensive interactions to the NADPH molecule bound in the neighboring binding cleft. For example, the Ser63 residue hydrogen bonds to the neighboring NADPH phosphate moiety via both main-chain amide and side-chain hydroxyl groups, the latter of which is inserted so as to form a bridged interaction between the cofactor and the Arg69 side chain from the host monomer. In addition, the Arg61 side chain is extended to form a direct hydrogen bond with the pyrophosphate bridge as well as a solvent-bridged interaction with the phosphate of the second NADPH. This places the Arg side chain in a position to simultaneously form protein−protein hydrogen bonds with the main-chain carbonyl oxygen atom of Ala115* as well as the side-chain hydroxyl of Ser117*.

In addition to the unique intermonomer contributions to cofactor binding, MUR1 also maintains a number of interactions with bound NADPH that are conserved with related enzymes. The Arg60 side chain packs against the planar surface of the adenine moiety while hydrogen bonding to the phosphate group, as has been observed for the GDP-fucose synthase (*17, 18*). Hydrogen bonding of the adenine by both the side chain of Asp91 and the main-chain amide group of the subsequent residue are also highly conserved interactions, both in $NAD^+$- and $NADP^+$-binding enzymes. The adenyl ribose forms direct hydrogen bonds with enzyme backbone via the free hydroxyl group with the amide nitrogen atoms of both Thr37 and Gly38. The Thr37 side chain also forms hydrogen bonds to both the ribose hydroxyl and phosphate moieties. The ribose ring oxygen is also within hydrogen-bonding distance of the main chain at the Ala115 amide nitrogen. These main-chain interactions are conserved in the structure of closely related GDP-L-fucose synthase (*17, 18*), which also utilizes $NADP^+$ rather than $NAD^+$.

In the region of the enzyme active site, one element of cofactor binding that is highly conserved among related enzymes is hydrogen bonding of the ribose hydroxyls by the Lys and Tyr side chains of the catalytic triad. Buried water molecules mediate additional interactions of the enzyme with one ribose hydroxyl as well as the pentose ring oxygen atom. The nicotinamide moiety of the cofactor is bound in a syn conformation, with the carboxyamide nitrogen within hydrogen-bonding distance of a phosphoryl oxygen atom. This conformation is consistent with NAD(P)H complexes of related enzymes and is the appropriate orientation for B-side hydride transfer during catalysis. The syn conformation may be further stabilized by hydrogen bonds with the surrounding MUR1 enzyme between the carboxyamide oxygen and His215 main-chain amide nitrogen as well as between ring hydrogen atoms and the carbonyl oxygen atoms of Gly161 and Leu212.

*Substrate Binding Site.* The MUR1 complexes presented here offer the first crystallographic observation of ligand binding among enzymes of this family that are specific for GDP-sugars. Moreover, the observation of a bound GDP-sugar (identified as GDP-D-rhamnose) in the active sites of three monomers in the type I crystals allows characterization of GDP-sugar interactions with MUR1. Binding interactions at the MUR1 substrate site are shown schematically in Figure 5 for GDP-D-rhamnose; however, the GDP moiety is bound identically in both GDP and GDP-D-rhamnose complexes. Interestingly, the GDP moiety binds in the syn conformation, whereas this nucleotide more typically binds to enzymes in the anti conformation. This conformation is stabilized by an intramolecular hydrogen bond between guanine amino nitrogen atom and phosphoryl oxygen atoms, with the N3 ring nitrogen atom also within hydrogen-bonding distance (3.1 Å) of the O5′ oxygen atom. The ability of GDP to adopt this unusual conformation may be an important determinant in substrate specificity for GMD enzymes.

The GDP moiety is bound entirely within the small domain of MUR1, with the pyrophosphate bridge hydrogen-bonding to the amide nitrogen of Val225, again at the positive dipole of an α-helix. This mode of substrate binding, reminiscent of dinucleotide binding by the Rossmann motif, appears as a common feature among closely related enzymes. GDP forms hydrogen bonds with the side chains of Asn214, Lys228, Arg253, Arg314, and Glu317 (Figure 5), residues

that are all highly conserved among the amino acid sequences of GMDs. Moreover, the hydrogen bonding of Arg314 to oxygen atoms of both phosphoryl groups and the hydrogen bonding of the carboxylate oxygens of Glu317 to either ribose hydroxyl group are interactions also observed in UDP-sugar binding SDR enzymes as well (*16*, *22*). The guanine ring hydrogen bonds to the MUR1 main chain at the Glu223 carbonyl and Gly247 amide groups. In addition to these direct protein/ligand hydrogen bonds, GDP also makes several interactions mediated by buried water molecules in the binding pocket.

In the type I crystal form, a GDP-sugar was observed in the substrate binding site for three monomers of the MUR1 tetramer, despite the absence of any added ligand in the crystallization experiments. Thus, a nucleotide-sugar from the expression host can remain tightly associated with the enzyme *throughout purification*. Similar behavior has previously been reported for GalE (*41*) and dTDP-D-glucose oxidoreductase (*32*), which were purified as naturally occurring abortive complexes because of tight binding of their cofactor and substrate/product. In the case of MUR1, the ligand observed in the binding site is most probably not the natural substrate, GDP-D-mannose, but rather GDP-D-rhamnose formed as a dead-end product during the overexpression of MUR1 in *E. coli*. Electron density for the sugar moiety (Figure 4) clearly indicates a single axial hydroxyl group at the O2 position, but no density is observed for an O6 hydroxyl group, consistent with D-rhamnose. Furthermore, analysis of the sugar content of the enzyme sample used for crystallization (data not shown) revealed the presence of GDP-rhamnose predominantly (87%), with lesser amounts of GDP-mannose.

D-Rhamnose is a rare sugar, thus far identified in nature only as a constituent of bacterial lipopolysaccharides. Only L-rhamnose has been detected in plant tissues; however, the formation of GDP-D-rhamnose in plant extracts has been known since the 1960s (*64*). In the presence of excess NADPH, MUR1 forms this product in the *E. coli* expression strain (*50*) by acting as a reductase on its natural 4-keto 6-deoxymannose product. The absence of detectable D-rhamnose in vivo suggests that these conversions by plant GMDs may be merely experimental artifacts; however, it remains possible, given the diverse range of carbohydrates produced by plants, that this unusual sugar may be a natural product formed only in low levels. Interestingly, the natural pathways of GDP-D-rhamnose biosynthesis have been elucidated for a number of bacterial species and are found to involve conversion of GDP-D-mannose in a two-step process, utilizing a homologous GDP-mannose dehydratase and second reductase enzyme (*65*). A GMD from *Aneurinibacillus thermoaerophilusthis* was similarly reported to catalyze both dehydratase and reductase reactions to produce a rhamnose product, albeit less efficiently than the natural reductase enzyme (*66*).

The presence of bound GDP-D-rhamnose provides an unexpected view of ligand binding, which should closely approximate that of the natural GDP-D-mannose substrate. The sugar moiety extends into the crevice between large and small domains of the MUR1 structure, where it is stabilized by extensive hydrogen-bonding interactions with the enzyme. At the catalytic center, the reactive O4 hydroxyl of the hexose moiety hydrogen bonds to the side chains of both Ser162 and Tyr185, residues of the catalytic site. The hexose O3 hydroxyl interacts with both Tyr185 and the main-chain carbonyl oxygen of Ser117, while the O5 ring oxygen is in good hydrogen-bonding distance to the Asn214 side-chain amino group. Specificity for the axial hydroxyl of the mannose substrate at the O2 position appears to be largely a result of steric hindrance by the adjacent Phe224 side chain (Figure 4a). In the GDP-D-rhamnose complex, the phenyl ring makes a van der Waals contact of 3.4 Å with C2 of the bound hexose and would be expected to obstruct binding of an equatorial hydroxyl at this position. A second important feature of binding appears to be the Arg220 side chain. Found in a parallel stacking arrangement with the Phe224 ring, Arg220 is positioned above the plane of the hexose ring, in good position to make stabilizing hydrogen bonds with an axial O2 hydroxyl group. The position of the Arg side chain itself is rigidly constrained by two hydrogen bonds with the Glu216 side chain as well as additional bonds to two buried water molecules, both of which interact simultaneously with NADPH pyrophosphate oxygen atoms.

Although not observed in the MUR1/GDP-D-rhamnose complex, the likely position of the O6 hydroxyl of the GDP-mannose can be reasonably deduced from the crystal structure. Two low-energy rotamer positions for the O6 hydroxyl are possible within the substrate binding site. One would place the hydroxyl within hydrogen-bonding distance of the side chain of Ser162, part of the catalytic triad; this orientation has previously been observed in the complex of SQD1 with UDP-glucose (*22*). However, this is the more sterically strained of the two orientations. It is more likely that the O6 hydroxyl adopts the second possible orientation, as is observed for UDP-glucose in GalE (*16*), which places it in position to hydrogen bond to both Ser163 and Asn214 side-chain oxygen atoms. In fact, a water molecule is found near this potential O6 position in the MUR1 complex, within 2.5 Å of the GDP-D-rhamnose C5 atom and making hydrogen-bonding contacts with the side chains of Ser163, Asn214, and Glu164. Notably, as discussed below, the latter residue is believed to serve as a catalytic base in the dehydratase reaction.

*Conformational Changes upon Ligand Binding.* In both GDP and GDP-D-rhamnose complexes, the conformation of the MUR1 enzyme is essentially identical, with a rmsd on main-chain atoms of 0.35 Å. Only a slight shift (0.5 Å) is observed in the small domain where loops 244−251 and 304−315 are more tightly closed over the bound substrate when GDP-D-rhamnose is the ligand. The structure of the substrate binding site itself as well as of the bound NADPH cofactor are also nearly indistinguishable in the two complexes. In the GDP complex, the ligand sugar moiety is replaced by four additional buried water molecules. One of these water molecules is found within 0.5 Å of the position occupied by the hexose O4 hydroxyl and makes identical hydrogen-bonding interactions, illustrating the strong driving force for binding at this position. The buried water molecule found near the presumed position of the mannose O6 hydroxyl group is conserved in the MUR1 complexes with both GDP-D-rhamnose and GDP but is shifted by 0.85 Å in the active site to accommodate the hexose moiety.

In contrast, the unoccupied MUR1 monomer in the asymmetric unit of the type I crystals reveals significant differences in the main-chain conformation. A comparison

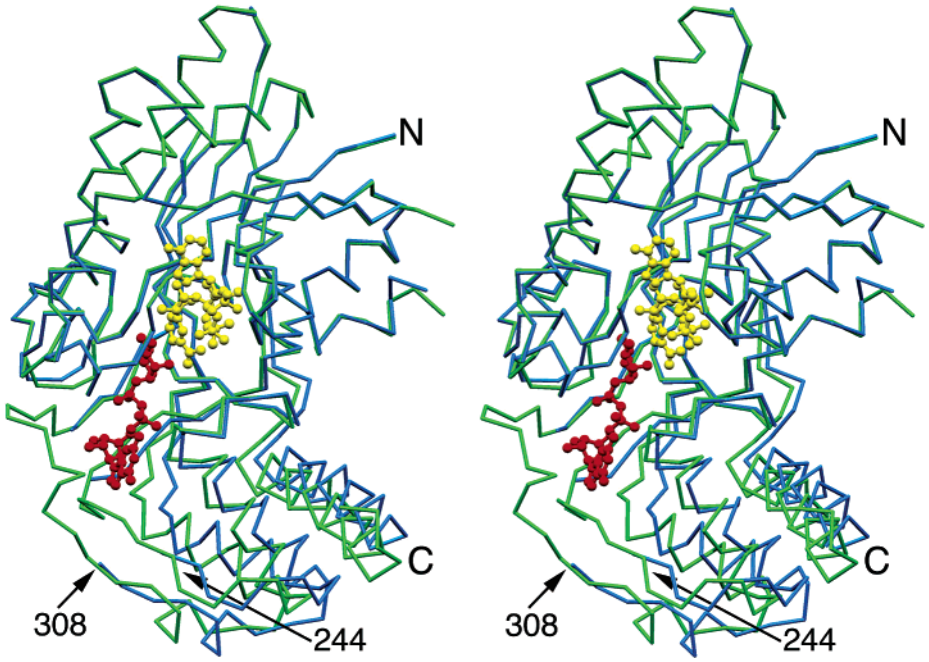


FIGURE 6: Superposition of MUR1 monomers in which substrate binding site is occupied (green) and empty (blue). Positions of bound NADPH (yellow) and GDP-D-rhamnose (red) ligands are depicted in ball-and-stick representation. When the substrate binding site is unoccupied, the small domain is shifted to a more open conformation, and two loops following residues 244 and 308 (arrows) are completely disordered. View is rotated approximately 90° from that of Figure 2a.

of monomers in bound and unbound states in shown in Figure 6. Although the large domain remains unchanged (rmsd of 0.45 Å on all atoms), the small domain of the unbound form has a more open conformation, with the helices shifted by up to 2.4 Å. Moreover, loops 245−250 and 309−318, which close over the bound ligand in the GDP and GDP-sugar complexes, are completely disordered and unobserved in electron density maps. Even when well-ordered in the MUR1 ternary complexes, these loops are not stabilized by hydrogen bonds with the rest of the protein structure but rather only by interactions with the bound ligand. Thus, these loops serve as flexible flaps that may open to allow access of substrate to the catalytic site; once the site is occupied, these loops in the closed conformation contribute important binding interactions and isolate the substrate from the surrounding solvent.

*Implications for Catalysis*. The SDR enzymes share a highly conserved catalytic triad of Y-XXX-K and Ser/Thr residues (*67*) and moreover appear to share a conserved general mechanism for the initiation of catalysis. The proposed mechanism for the MUR1 reaction (*68*) is shown schematically in Figure 1. In the first step, common to all SDR enzymes, the deprotonation of the O4 hydroxyl by a general base, coupled with concerted hydride abstraction from the C4 atom by the $NAD(P)^+$ cofactor, yields a 4-keto intermediate (2). The MUR1 reaction then proceeds by elimination of a water molecule from C6, yielding a 4-keto-5,6-ene species (3), followed by reduction of the C5−C6 double bond to form the final 4-keto-6-deoxymannose product (4). This mechanism is supported by the recent detection of a 4-keto-5,6-glucoseen intermediate for the homologous dTGDH reaction (*34*). It has been demonstrated for a bacterial GMD (*68*) as well as for dTGDH (*33*) that it is the mannose C4 hydride that is transferred via NADPH to C6 in the final reduction step.

The importance of the Tyr, Lys, Ser/Thr triad for catalysis has been demonstrated by mutagenesis and kinetic studies for *E. coli* GMD (*23*) as well as for other related SDR enzymes. The Tyr side chain, in the form of a negatively charged tyrosinate, has been identified as the catalytic base that acts on the reactive substrate O4 hydroxyl. In the MUR1 complex, a hydrogen bond between the phenolic oxygen of Tyr185 and the rhamnose O4 hydroxyl implies the direct attack on O4 by the Tyr base during catalysis, consistent with similar results derived from the recent crystal structures of SQD1 (*22*), GalE (*28*), dTGDH (*35*), and RmlB (*31*). The adjacent Lys side chain in the SDR triad is believed to serve in modifying the Tyr $pK_a$, stablizing the negative charge of the tyrosinate moiety, as well as contributing to cofactor binding (*36*, *69*, *70*). The role of the conserved Ser/Thr is less clearly defined. The Ser/Thr side chain may play a role in the proper orientation of bound substrate and/or in the stabilization of reaction intermediates or transition states. Unusually short (<2.5 Å) hydrogen bonds between this side chain and the hexose O4 hydroxyl were noted for the productive ternary complex in SQD1 (*22*) and the abortive complexes of GalE (*28*) and Rm1B (*31*). The presence of short, low-barrier hydrogen bonds at this position has been proposed to facilitate proton transfer during catalysis (*21*, *22*, *28*). The average hydrogen-bonding distance of 2.4 Å between hexose O4 and Ser hydroxyl groups in the MUR1 complex is consistent with these observations.

It has recently been proposed for the broader class SDR enzymes that the catalytic triad should be expanded to a tetrad, including as well a highly conserved Asn residue (*71*). For these enzymes, the Asn backbone carbonyl is postulated to participate in a proton relay involving the catalytic Lys and Tyr side chains, a cofactor ribose hydroxyl, and a pocket of buried water molecules, thus facilitating proton transfer and serving as a bridge for exchange between the catalytic site and the bulk solvent. Although the corresponding position is substituted by a Val residue in the MUR1 structure, a solvent-bridged interaction is maintained between

the main-chain carbonyl oxygen and the catalytic Lys side chain. However, unlike the more distant SDR relatives, in the complexes of MUR1 and most other closely related enzymes, the catalytic Lys and Tyr side chains are not directly networked via mutual hydrogen bonding to a common NAD(P) ribose hydroxyl (Figure 5), as required by the proton relay hypothesis.

In addition to the highly conserved triad, the dehydratase reaction requires a general base to accept the C5 hydrogen from the 4-keto intermediate in the second step of catalysis. This proton is later returned to the substrate in the final step of catalysis. Mutagenesis experiments with the GMD from *E. coli* (*23*) as well as the structurally and mechanistically homologous dTGDH (*37*) have identified a conserved Glu residue in the active site that serves this function. The corresponding residue in the MUR1 enzyme, Glu164, is positioned nearly directly under and 3.9 Å from the C5 atom of bound hexose in the GDP-D-rhamnose complex. Modest torsional rotations of the side chain could easily bring the Glu164 carboxylate within a distance suitable for proton abstraction. Apart from potential interactions with the substrate hexose moiety described above, the Glu164 side chain makes the most direct contacts in the ternary complex with the GDP pyrophosphate bridge. The Glu164 carboxylate OE1 atom, which is oriented most appropriately for interaction with the hexose, is also within 3.6 Å of one phosphoryl oxygen, while the OE2 oxygen makes a bridged hydrogen-bonding interaction with a second phosphoryl oxygen via a buried water molecule. The latter solvent-bridged interaction is part of a hydrogen-bonding network involving the Glu OE2 atom and four buried water molecules arranged in a pentagonal geometry. Glu164 is otherwise surrounded in the MUR1 binding site by the hydrophobic side chains of Val119, Val318, and Leu321 and makes hydrogen bonds only with a cavity of buried water molecules. The hydrogen-bonding network of Glu164 with the pyrophosphate, the latter in turn simultaneously hydrogen bonded by Arg253, may be an important influence on its catalytic role as both a proton acceptor and a proton donor.

The dehydration step also requires, in addition to a general base, an acid responsible for protonation of the O6 hydroxyl group to release a water molecule. In the case of dTGDH, mutagenesis experiments suggest that an active site Asp residue serves as this acid (*37*). In the MUR1 structure, the corresponding residue, Ser163, is in good hydrogen-bonding distance (2.8 Å) to the assumed mannose O6 position and may also reasonably serve this role. However, in this position the O6 hydroxyl is simultaneously in good hydrogen-bonding distance to Asn214 (~2.5 Å) and is approximately 3 Å from Glu164 in its observed conformation. Thus, based on the MUR1 crystal structure, it remains possible that the catalytic Glu164 may simultaneously act as both base and acid in the dehydration step, as previously proposed by Hegeman et al. (*35*) for related dehydratases.

Among enzymes of this SDR subfamily, a distinguishing feature of the dehydratase reaction is the intramolecular hydride transfer from C4 to C6. This clearly requires a change in the relative orientations of the hexose and nicotinamide rings so that both substrate carbon centers may be appropriately positioned during the course of catalysis. The MUR1 ternary complex with NADPH and GDP-D-rhamnose most closely resembles the reaction complex at the final stage of catalysis, when the reduced cofactor and 4-keto 5,6-ene intermediate are poised for hydride transfer. In the crystal structure, the reactive nicotinamide C4 atom of NADPH is nearly aligned with the rhamnose C6 atom at a distance of 3.4 Å, within the range expected for hydride transfer. The observed position of the rhamnose ring within the MUR1 site is probably representative of the mannose substrate, as it is nearly identical to that of the natural substrate glucose moiety in the dTGDH complex when the two active sites are superimposed. Allard et al. (*31*) have proposed for the latter enzyme that a significant rearrangement of the hexose moiety may be driven by steric repulsion with the water molecule released during catalysis. On the basis of the MUR1 complex, it appears that even a modest rotation in the hexose orientation would bring the C6 atom in excellent position to allow hydride transfer (Figure 4). In fact, the buried water molecule observed within 2.5 Å of the hexose C5 atom suggests that a large adjustment in the substrate orientation may not be required in MUR1.

For the initial hydride abstraction at the hexose C4 position, the necessary changes in alignment of substrate and cofactor probably result primarily from rotations of the nicotinamide ring that may accompany changes in oxidation state. The active site is quite sterically constrained in the region of the cofactor. Hence, the planar nicotinamide ring of the oxidized cofactor would make unacceptably close contacts with the neighboring Arg220 side chain (2.3 Å), as well as the O2 hydroxyl (2.2 Å) of the substrate itself, without some conformational adjustments.

*Structural Indications of Negative Cooperativity*? The observation of a single unoccupied substrate binding site in the tetrameric MUR1/NADPH/GDP-D-rhamnose complex raises the intriguing possibility that the subunits exhibit distinctly different affinities toward GDP-D-rhamnose and perhaps other GDP-sugars. Having a mix of occupied and unoccupied active sites in a symmetric oligomer is not an uncommon observation in crystal structures and does not suggest, a priori, negative cooperativity. However, all of the GDP-D-rhamnose in the MUR1 preparation originated from the *E. coli* expression host and was retained throughout enzyme purification, sample concentration, and buffer exchange by virtue of its affinity to MUR1. With essentially no free GDP-D-rhamnose remaining in the MUR1 preparation, a stable MUR1/NADPH/GDP-D-rhamnose complex with a single, unoccupied active site most likely existed prior to crystallization. When millimolar concentrations of GDP and other GDP-sugars (e.g., GDP-D-mannose) are used in cocrystallization experiments, only a symmetric MUR1 tetramer with all substrate binding sites uniformly occupied is observed (A. M. Mulichak and R. M. Garavito, unpublished observations). Moreover, these other MUR1 complexes crystallize in either the type I ($P2_12_12_1$) or the type II ($C222_1$) crystal forms. The packing within both crystal lattices is surprisingly equivalent, and there is also no indication that crystal contacts would impede substrate binding. This is particularly true for the type I crystal form where the "unoccupied" subunit merely swings closed under saturating concentrations of a GDP-D-mannose (A. M. Mulichak and R. M. Garavito, unpublished observations). Thus, the "unoccupied" subunit in the MUR1/NADPH/GDP-D-rhamnose complex must have an intrinsically lower affinity toward the GDP-sugar than the other three.

While a detailed structural basis for lower binding affinity for GDP-D-rhamnose is not immediately apparent, contacts exist between neighboring monomers that could mediate such communication between the substrate-binding domains. For instance, across the tetramer interface, the long C-terminal helices from the small domains of adjacent monomers pack against one another (Figure 2b). This interaction is significantly perturbed in the case of the single unoccupied monomer. Additionally, close contacts occur between segments 169−182 of monomers related by the highly conserved back-to-back dimer interface. These loops contribute to a small section of $\beta$-sheet including three $\beta$-strands of the small domain, all of which are shifted in response to the binding of substrate.

In summary, the X-ray crystal structures of MUR1 complexes presented here confirm the presence of catalytic residues that are conserved among the sequences of related enzyme and further suggest residues that are likely determinants in substrate binding and specificity. Beyond this, however, the structures present unexpected and intriguing issues, including the syn binding mode of GDP, the functional role of tetrameric GMD, and the possible existence of negative cooperativity, which all warrant further investigation. Efforts also continue toward successful displacement of tightly bound NADPH in the purified enzyme to address issues such as the effect of cofactor oxidation state on active site conformation and the role of NADP(H) binding in tetramer formation.

## ACKNOWLEDGMENT

We gratefully acknowledge M. Dumond for preparation and purification of the MUR1 enzyme. Studies related here were supported by the U.S. Department of Energy Grant DE-FG02-95ER20203 (W.-D.R.) and the Michigan Life Science Corridor grant to the Center for Structural Biology (R.M.G.). Research was carried out in part at the National Synchrotron Light Source, Brookhaven National Laboratory, which is supported by the U.S. Department of Energy. Portions of this work were performed at the DuPont-Northwestern-Dow Collaborative Access Team (DND-CAT) Synchrotron Research Center located at Sector 5 of the Advanced Photon Source (APS). DND-CAT is supported by E.I. DuPont de Nemours & Co., Dow Chemical Company, NSF Grant DMR-9304725, and a grant from the State of Illinois (IBHE HECA NWU 96). Use of the Argonne National Laboratory Structural Biology Center 19ID beamline at the APS was supported by the U.S. Department of Energy, under Contract W-31-109-ENG-38. We thank the staffs of the NSLS X25 and APS DND and SBC beamlines for their assistance.

## REFERENCES

1. Varki, A. (1994) *Proc. Natl. Acad. Sci. U.S.A. 91*, 7390−7497.
2. Roos, C., Kolmer, M., Mattila, P., and Renkonen, R. (2001) *J. Biol. Chem. 277*, 3168−3175.
3. Lamrabet, Y., Bellogin, R. A., Cubo, T., Espuny, R., Gil, A., Krishnan, H. B., Megias, M., Ollero, F. J., Pueppke, S. G., Ruiz-Sainz, J. E., Spaink, H. P., Tejero-Mateo, P., Thomas-Oates, J., and Vinardell, J. M. (1999) *Mol. Plant-Microbe Interact. 12*, 207−217.
4. Lopez-Lara, I. M., Blok-Tip, L., Quinto, C., Garcia, M. L., Bloemberg, G. V., Lamers, G. E., Lugtenberg, B. J., Thomas-Oates, J., and Spaink, H. P. (1996) *Mol. Microbiol. 21*, 397−408.
5. Levy, S., York, W. S., Stuike-Prill, R., Meyer, B., and Staehelin, L. A. (1991) *Plant J. 1*, 195−215.
6. Levy, S., Maclachlan, G., and Staehelin, L. A. (1997) *Plant J. 11*, 373−386.
7. Vanzin, G. F., Madson, M., Carpita, N. C., Raikhel, N. V., Keegstra, K., and Reiter, W.-D. (2002) *Proc. Natl. Acad. Sci. U.S.A. 99*, 3340−3345.
8. O'Neill, M. A., Eberhard, S., Albersheim, P., and Darvill, A. G. (2001) *Science 294*, 846−849.
9. Baker, M. E., and Blasco, R. (1992) *FEBS Lett. 301*, 89−93.
10. Labesse, G., Vidal-Cros, A., Chomilier, J., Gaudry, M., and Mornon, J.-P. (1994) *Biochem. J. 304*, 95−99.
11. Krozowski, Z. (1994) *J. Steroid Biochem. Mol. Biol. 51*, 125−130.
12. Jornvall, H., Persson, B., Krook, M., Atrian, S., Gonzalez-Duarte, R., Jeffery, J., and Ghosh, D. (1995) *Biochemistry 34*, 6003−6013.
13. Jornvall, H., Hoog, J.-O., and Persson, B. (1999) *FEBS Lett. 445*, 261−264.
14. Bauer, A. J., Rayment, I., Frey, P. A., and Holden, H. M. (1992) *Proteins 12*, 372−381.
15. Thoden, J. B., Frey, P. A., and Holden, H. M. (1996) *Protein Sci. 5*, 2149−2161.
16. Thoden, J. B., Frey, P. A., and Holden, H. M. (1996) *Biochemistry 35*, 5137−5144.
17. Somers, W. S., Stahl, M. L., and Sullivan, F. X. (1998) *Structure 6*, 1601−1612.
18. Rizzi, M., Tonetti, M., Vigevani, P., Sturla, L., Bisso, A., De Flora, A., Bordo, D., and Bolognesi, M. (1998) *Structure 6*, 1453−1465.
19. Allard, S. T. M., Giraud, M.-F., Whitfield, C., Graninger, M., Messner, P., and Naismith, J. H. (2001) *J. Mol. Biol. 307*, 283−295.
20. Deacon, A. M., Ni, Y. S., Coleman, W. G., Jr., and Ealick, S. E. (2000) *Structure 8*, 453.
21. Blankenfeldt, W., Kerr, I. D., Giraud, M.-F., McMiken, H. J., Leonard, G. A., Whitfield, C., Messner, P., Graninger, M., and Naismith, J. H. (2002) *Structure 10*, 773−786.
22. Mulichak, A. M., Theisen, M. J., Essigmann, B., Benning, C., and Garavito, R. M. (1999) *Proc. Natl. Acad. Sci. U.S.A. 96*, 13097−13102.
23. Somoza, J. R., Menon, S., Schmidt, H., Joseph-McCarthy, D., Dessen, A., Stahl, M. L., Somers, W. S., and Sullivan, F. X. (2000) *Structure 8*, 123−135.
24. Thoden, J. B., Frey, P. A., and Holden, H. M. (1996) *Biochemistry 35*, 2557−2566.
25. Thoden, J. B., Gulick, A. M., and Holden, H. M. (1997) *Biochemistry 36*, 10685−10695.
26. Thoden, J. B., Hegeman, A. D., Wesenberg, G., Chapeau, M. C., Frey, P. A., and Holden, H. M. (1997) *Biochemistry 36*, 6294−6304.
27. Thoden, J. B., and Holden, H. M. (1998) *Biochemistry 37*, 11469−11477.
28. Thoden, J. B., Wohlers, T. M., Fridovich-Keil, J. L., and Holden, H. M. (2000) *Biochemistry 39*, 5691−5701.
29. Thoden, J. B., Wohlers, T. M., Fridovich-Keil, J. L., and Holden, H. M. (2001) *J. Biol. Chem. 276*, 20617−20623.
30. Thoden, J. B., Wohlers, T. M., Fridovich-Keil, J. L., and Holden, H. M. (2001) *J. Biol. Chem. 276*, 15131−15136.
31. Allard, S. T. M., Beis, K., Giraud, M.-F., Hegeman, A. D., Gross, J. W., Wilmouth, R. C., Whitfield, C., Graninger, M., Messner, P., Allen, A. G., Maskell, D. J., and Naismith, J. H. (2002) *Structure 10*, 81−92.
32. Zarkowsky, H., Lipkin, E., and Glaser, L. (1970) *J. Biol. Chem. 245*, 6599−6606.
33. Snipes, C. E., Brillinger, G.-U., Sellers, L., Mascaro, L., and Floss, H. G. (1977) *J. Biol. Chem. 252*, 8113−8117.
34. Gross, J. W., Hegeman, A. D., Vestling, M. M., and Frey, P. A. (2000) *Biochemistry 39*.
35. Hegeman, A. D., Gross, J. W., and Frey, P. A. (2001) *Biochemistry 40*, 6598−6610.
36. Gerratana, B., Cleland, W. W., and Frey, P. A. (2001) *Biochemistry 40*, 9187−9195.
37. Gross, J. W., Hegeman, A. D., Gerratana, B., and Frey, P. A. (2001) *Biochemistry 40*, 12497−12504.
38. Hegeman, A. D., Gross, J. W., and Frey, P. A. (2002) *Biochemistry 41*, 2797−2804.
39. Berger, E., Arabshahi, A., Wei, Y., Schilling, J. F., and Frey, P. A. (2001) *Biochemistry 40*, 6699−6705.

40. Liu, Y., Thoden, J. B., Kim, J., Berger, E., Gulick, A. M., Ruzicka, F. J., Holden, H. M., and Frey, P. A. (1997) *Biochemistry 36*, 10675−10684.
41. Vanhooke, J. L., and Frey, P. A. (1994) *J. Biol. Chem. 269*, 31496−31504.
42. Liu, Y., Vanhooke, J. L., and Frey, P. A. (1996) *Biochemistry 35*, 7615−7620.
43. Swanson, B. A., and Frey, P. A. (1993) *Biochemistry 32*, 13231−13236.
44. Burke, J. R., and Frey, P. A. (1993) *Biochemistry 32*, 13220−13230.
45. Flentke, G. R., and Frey, P. A. (1990) *Biochemistry 29*, 2430−2436.
46. Arabshahi, A., Flentke, G. R., and Frey, P. A. (1988) *J. Biol. Chem. 263*, 2638−2643.
47. Wee, T. G., Davis, J., and Frey, P. A. (1972) *J. Biol. Chem. 247*, 1339−1342.
48. Wee, T. G., and Frey, P. A. (1973) *J. Biol. Chem. 248*, 33−40.
49. Wong, S. S., and Frey, P. A. (1977) *Biochemistry 16*, 298−305.
50. Bonin, C. P., Potter, I., Vanzin, G. F., and Reiter, W.-D. (1997) *Proc. Natl. Acad. Sci. U.S.A. 94*, 2085−2090.
51. Zablackis, E., York, W. S., Pauly, M., Hantus, S., Reiter, W.-D., Chapple, C. C. S., Albersheim, P., and Darvill, A. G. (1996) *Science 272*, 1808−1810.
52. Reiter, W.-D., Chapple, C. C. S., and Somerville, C. R. (1993) *Science 261*, 1032−1035.
53. Jancarik, J., and Kim, S.-H. (1991) *J. Appl. Crystallogr. 24*, 409−411.
54. Otwinowski, Z., and Minor, W. (1997) *Methods Enzymol. 276*, 307−326.
55. Brunger, A. T. (1998) *Acta Crystallogr. D54*, 905−921.
56. CHAIN (1995) *CHAIN*: *Crystallographic Modeling Program Version 7.0*, Baylor College of Medicine, Waco, TX.
57. Navaza, J. (1994) *Acta Crystallogr. A50*, 157−163.
58. Collaborative Computational Project N. (1994) *Acta Crystallogr. D50*, 760−763.
59. Rossmann, M. G., Liljas, A., Branden, C.-I., and Banaszak, L. J. (1975) *Enzymes 11*, 61−102.
60. Bisso, A., Sturla, L., Zanardi, D., De Flora, A., and Tonetti, M. (1999) *FEBS Lett. 456*, 370−374.
61. Wu, B., Zhang, Y., and Wang, P. G. (2001) *Biochem. Biophys. Res. Commun. 285*, 364−371.
62. Broschat, K. O., Chang, S., and Serif, G. (1985) *Eur. J. Biochem. 153*, 397−401.
63. Sturla, L., Bisso, A., Zanardi, D., Benatti, U., De Flora, A., and Tonetti, M. (1997) *FEBS Lett. 412*, 126−130.
64. Barber, G. A. (1968) *Biochim. Biophys. Acta 165*, 68−75.
65. Rocchetta, H. L., Pacan, J. C., and Lam, J. S. (1998) *Mol. Microbiol. 29*, 1419−1434.
66. Kneidinger, B., Graninger, M., Adams, G., Puchberger, M., Kosma, P., Zayni, S., and Messner, P. (2001) *J. Biol. Chem. 276*, 5577−5583.
67. Persson, B., Krook, M., and Jornvall, H. (1991) *Eur. J. Biochem. 200*, 537−543.
68. Oths, P. J., Mayer, R. M., and Floss, H. G. (1990) *Carbohydr. Res. 198*, 91−100.
69. Varughese, K. I., Xuong, N. H., Kiefer, P. M., Matthews, D. A., and Whiteley, J. M. (1994) *Proc. Natl. Acad. Sci. U.S.A. 91*, 5582−5586.
70. Winberg, J. O., Brendskag, M. K., Sylte, I., Lindstad, R. I., and McKinley-McKee, J. S. (1999) *J. Mol. Biol. 294*, 601−616.
71. Filling, C., Berndt, K. D., Benach, J., Knapp, S., Prozorovski, T., Nordling, E., Ladenstein, R., Jornvall, H., and Oppermann, U. (2002) *J. Biol. Chem. 277*, 25677−25684.
72. Kraulis, P. J. (1991) *J. Appl. Crystallogr. 24*, 946−950.
73. Merrit, E., and Murphy, M. (1994) *Acta Crystallogr. D50*, 869−873.
74. Evans, S. V. (1993) *J. Mol. Graphics 11*, 134−138.

BI0266683